Materials Research. 2025; 28(suppl. 1): e20250046
DOI: https://doi.org/10.1590/1980-5373-MR-2025-0046

PLA/PHBV/SEP/ZnO Hybrid Composites for Antimicrobial Multifunctional Packaging

***Aline Vasconcelos Duarte*[a*], *Herich Luan Lopes*[b], *Bruno Carlucci Stefanelli de Luca*[b], *Mateus Gonçalves Prado Balado*[c], *Ana Beatriz Klosowski*[c], *Juliana Bonametti Olivato*[c], *Rosario Elida Suman Bretas*[b], *Fabio Roberto Passador*[d], *Francys Kley Vieira Moreira*[a,b], *Juliano Marini*[a,b]**

[a] *Universidade Federal de São Carlos (UFSCar), Programa de Pós-Graduação em Ciência e Engenharia de Materiais (PPGCEM), Rod. Washington Luís, km 235, 13565-905, São Carlos, SP, Brasil.*
[b] *Universidade Federal de São Carlos (UFSCar), Departamento de Engenharia de Materiais (DEMa), Rod. Washington Luís, km 235, 13565-905, São Carlos, SP, Brasil.*
[c] *Universidade Estadual de Ponta Grossa (UEPG), Departamento de Ciências Farmacêuticas (DEFAR), Av. Carlos Cavalcanti, 4748, 84030-900, Ponta Grossa, PR, Brasil.*
[d] *Universidade Federal de São Paulo (UNIFESP), Laboratório de Tecnologia de Polímeros e Biopolímeros (TecPBio), Rua Talim, 330, 12231-280, São José dos Campos, SP, Brasil.*

Received: January 08, 2025; Revised: August 01, 2025; Accepted: August 14, 2025

The development of multifunctional packaging addresses the demand for solutions that combine protection, sustainability, and functionalities such as antimicrobial activity. In this context, films of hybrid composites (HC) based on a poly(lactic acid)/poly(3-hydroxybutyrate-*co*-3-hydroxyvalerate) blend - PLA/PHBV (70/30 wt/wt), sepiolite nanoparticles (SEP, 5 phr), and different contents (3 and 5 phr) of micrometric zinc oxide (ZnO) were produced via melt mixing and compression molding. The influence of ZnO content on rheological, thermal, mechanical, and water vapor permeability properties, as well as its role as an antimicrobial agent, was evaluated. Despite ZnO acting as a catalyst for PLA degradation during processing, the HC with 3 phr of ZnO demonstrated significant improvements, including a 16% in elastic modulus and a 21% increase in tensile strength (compared to PLA/PHBV blend), an 85% reduction in water vapor permeability (compared to PLA/PHBV/SEP nanocomposite), good processability, and effective inhibition of bacterial growth on the film surface. These results highlight the potential of HC with 3 phr of ZnO for producing multifunctional packaging using conventional melt-processing techniques.

Keywords: *Packaging, hybrid composites, antimicrobial, poly(lactic acid), poly(3-hydroxybutyrate-co-3-hydroxyvalerate).*

1. Introduction

The development of multifunctional packaging that aligns with global trends in the food and healthcare sectors has garnered increasing attention from researchers and industry professionals. Such packaging not only needs to exhibit adequate physical properties (such as barrier, mechanical, optical, and thermal properties) but also enhanced functionalities, including biodegradability and antimicrobial activity[1]. Furthermore, the use of non-biodegradable, petroleum-derived polymers in short-lifecycle applications, combined with inadequate solid waste management and improper disposal practices, has significantly worsened the environmental challenges caused by plastic pollution[2].

In this context, biodegradable polymers derived from renewable sources, such as poly(lactic acid) (PLA) and poly(3-hydroxybutyrate-*co*-3-hydroxyvalerate) (PHBV), emerge as promising alternatives. PLA offers several advantages, including good processability and mechanical properties comparable to petrochemical-derived polymers. However, its brittle nature, high glass transition temperature (T_g), and slow degradation kinetics limit its range of applications[3]. The development of polymer blends with PHBV presents a viable strategy to enhance PLA's performance, as PHBV can improve water vapor and oxygen barrier properties while modifying PLA´s degradation behavior[4].

To optimize the technological performance of this immiscible blend, different compatibilization and reinforcement strategies can be applied. Among the main approaches reported in the literature for polymer blends compatibilization are the addition of block or graft copolymers, reactive polymers, and, more recently, the selective dispersion of nanoparticles[5,6]. Nanoparticles can localize within the matrix, the second phase, and/or the interface, making this strategy particularly promising[5,6]. This approach not only reduces interfacial energy and inhibits coalescence, but also modifies the viscosity ratio

* e-mail: alinevd@estudante.ufscar.br
Associate Editor: Leonardo Gondim de Andrade e Silva.
Editor-in-Chief: Luiz Antonio Pessan.

of the blend. Furthermore, nanoparticles can also provide significant reinforcement effects, particularly when present in sufficient quantity and dispersion state to form a percolated network of physical interactions[7].

Sepiolite (SEP) is a clay mineral with the chemical formula $Si_{12}O_{30}Mg_8(OH)_4(H_2O)_4 \cdot 8H_2O$. Its structure consists of alternating blocks and tunnels that grow in the fibrous direction. Each structural block consists of two tetrahedral silica layers and a central octahedral layer containing magnesium[8,9]. Its needle-like geometry, high surface area (300 - 400 m^2/g), and availability of surface hydroxyl (-OH) groups[10,11] make it an excellent candidate as both a compatibilizer and reinforcing agent for polyesters. Studies have demonstrated its positive effects when incorporated into PLA nanocomposites, including altered crystallization behavior[12], flame retardancy[13], improved thermal and mechanical properties[14,15], enhanced rheological behavior[16], and accelerated biodegradation in soil[17]. There are also reports of SEP´s incorporation into PHBV nanocomposites, resulting in improvements in thermal and mechanical properties[18], water vapor permeability and biodegradability[19], and the release kinetics of oregano essential oil in active packaging[20,21].

Only a few studies[22,23] have investigated nanocomposites based on PHBV/PLA blends and sepiolite, with none focusing on PLA/PHBV/SEP composites where PLA is the predominant polymer phase (i.e., the matrix). González-Ausejo et al.[22] evaluated the incorporation of varying SEP contents (1 - 4 phr) into a PHBV/PLA blend (75/25 wt/wt) via twin-screw extrusion followed by injection molding. Their results demonstrated improved compatibility between the biopolymers, a 15% reduction in oxygen permeability, and increased stiffness and elongation at break. Zembouai et al.[23] produced PHBV/PLA (50/50 wt/wt) nanocomposites containing SEP, Cloisite 30B (organically modified montmorillonite), and hybrid nanocomposites with both nanoparticles through melt blending followed by compression molding of films. The authors observed more effective compatibilization in hybrid nanocomposites, which results in more homogeneous and regular blend morphologies, as well as enhanced thermal stability and mechanical properties, including increased stiffness and hardness.

Antimicrobial packaging is designed to inhibit or delay the growth of microorganisms, extending product shelf life and ensuring greater consumer safety[24]. Numerous studies have reported the development of antimicrobial packaging based on PLA[25], PHBV[26], and PLA/PHBV blends[27,28], incorporating a wide variety of potential active agents, such as essential oils (e.g., oregano[20] and thyme[29]), plant extracts (e.g.,tannins[30]), inorganic agents (Ag^+ and Cu^{2+} ions[30]), metal oxides (ZnO and TiO_2[30]), and carbon materials (graphene nanoplatelets[27] and carbon nanotubes[27,28]). Zinc oxide (ZnO) stands out for its proven antimicrobial activity and high thermal stability, making it suitable for use in conventional thermoplastic processing methods[31]. Additionally, ZnO has been studied as an additive to enhance PLA degradability[32] and recycling[33], acting as a catalyst in the degradation process, with nanoscale ZnO showing greater effectiveness[34].

Therefore, this study proposes the development of hybrid composites based on PLA/PHBV/SEP/ZnO, targeting potential applications in biodegradable and antimicrobial multifunctional packaging. The inclusion of varying amounts of micrometric ZnO was analyzed, aiming to balance its antimicrobial action with its impact on the degradation of the PLA matrix during melt-state processing, ensuring levels that preserve both the processability and the technological performance of the developed materials.

2. Materials and Methods

2.1. Materials

The following materials were used to produce the hybrid composites: i) poly(lactic acid) (PLA), Ingeo Biopolymer 4043D from NatureWorks (USA), with a density of 1.24 g/cm^3, a melt flow index of 6 g/10 min (210 °C/2.16 kg), and an estimated D,D-lactide isomer content of approximately 5 wt%[35,36]; ii) poly(3-hydroxybutyrate-*co*-3-hydroxyvalerate) (PHBV), PHI 002 from NaturePlast (France), with a density of 1.25 g/cm^3, a melt flow index between 15 and 30 g/10 min (190 °C/2.16 kg), and an estimated hydroxyvalerate (HV) content of 2 wt%[27]; iii) sepiolite (SEP), product #70253 from Sigma-Aldrich (USA), with a magnesium content of approximately 13 wt% and a mass loss on drying of less than 10 wt%; iv) zinc oxide (ZnO): product #205532 from Sigma-Aldrich (USA), with a particle size of less than 5 µm and a purity of 99.9 wt%.

2.2. Processing

Before processing the samples, all materials were dried in an air-circulation oven (model TE-394/2 from Tecnal Equipamentos Científicos) at 60 °C for at least 12 h.

To obtain the samples, an internal mixer HAAKE (model Rheomix 600p), equipped with roller-type rotors, was used at 180 °C, with a rotation speed of 100 rpm and a total mixing time of 10 minutes. Four formulations were produced, named and described as shown in Table 1.

To produce the PLA/PHBV blend (B), both polymers were simultaneously fed into the mixing chamber. The PLA/PHBV/SEP nanocomposite (N) was produced using a two-step process: first, a PHBV/SEP masterbatch was prepared

Table 1. Description of the samples produced.

Sample	PLA (phr)*	PHBV (phr)	SEP (phr)	ZnO (phr)	Description
B	70	30	---	---	PLA/PHBV blend
N	70	30	5	---	PLA/PHBV/SEP nanocomposite
HC3	70	30	5	3	PLA/PHBV/SEP/ZnO hybrid composite
HC5	70	30	5	5	PLA/PHBV/SEP/ZnO hybrid composite

* phr = parts per hundred of resin

with a mixing time of 5 minutes, followed by its dilution in the PLA matrix for an additional 5 minutes of mixing. This mixing protocol was designed to promote the preferential location of SEP nanoparticles at the interface of the PLA/PHBV blend, enhancing their role as both reinforcing and compatibilizing agents for the immiscible blend. The PLA/PHBV/SEP/ZnO hybrid composites (HC), with varying ZnO contents, were prepared using the same mixing protocol as for sample N. However, the ZnO particles were incorporated during the dilution step of the PHBV/SEP masterbatch in the PLA matrix.

Subsequently, films of all formulations were produced through compression molding using a MA098/A hydraulic press from Marconi Equipamentos para Laboratórios. The process was conducted at 180 °C, following a thermal cycle consisting of 2 minutes of preheating, 1 minute at an applied pressure of 1 ton, 1 minute at 3 tons, and 2 minutes at 5 tons, with pressure relief between each pressing cycle. After the forming process, the films were cut into specific shapes according to the requirements of subsequent characterization procedures.

2.3. Characterizations

2.3.1. Morphology

Ultrathin films were obtained from the materials processed in the internal mixer using a cryo-ultramicrotome (Reichert Ultracut FC4 model, Leica). Sectioning was performed below the glass transition temperature (T_g) of the polymers, with the knife set at -30 °C and the chamber temperature at -20 °C. Subsequently, the films were analyzed using a FEI Magellan 400L FEG-SEM microscope equipped with scanning transmission electron microscopy (STEM) detectors, operated at 30 kV and 25 pA.

2.3.2. Rheology

The rheological behavior of the materials obtained after the mixing process was analyzed under steady state (viscosity, η, as a function of shear rate, $\dot{\gamma}$, ranging from 0.01 to 100 s^{-1}) and oscillatory (storage modulus, G', and loss modulus, G'', as a function of oscillation frequency, ω, ranging from 0.02 to 100 rad/s, applying a strain amplitude within the linear viscoelastic region) regimes. The analyses were conducted using a controlled stress rheometer (model ARG2, TA Instruments) equipped with a parallel plate geometry, with a plate diameter of 25 mm, a 1 mm gap between the plates, at a temperature of 180 °C.

2.3.3. X-Ray diffraction (XRD)

The compression molded films and pure SEP and ZnO were structurally characterized by X-ray diffraction (XRD) using a Bruker D8 Advance Eco diffractometer with CuK_α radiation (25 mA, 40 kV). The analyses were performed with 2θ scanning from 5° to 90° and a step size of 0.02°.

2.3.4. Thermal characterization

The thermal decomposition behavior of the samples was analyzed by thermogravimetry (TGA), using a Q50 device from TA Instruments, under heating at a rate of 20 °C/min, from room temperature to 800 °C, in a nitrogen atmosphere.

The thermal behavior during the first DSC (differential scanning calorimetry) heating cycle of the samples was evaluated using a TA Instruments equipment, model Q2000, with nitrogen as carrier gas (50 mL/min), heating from 30 to 200 °C at a heat rate of 10 °C/min. Equation 1 was used to calculate the degree of crystallinity ($X_{c,i}$) of the PLA and PHBV phases:

$$X_{c,i} = \left(\frac{\Delta H_{m,i} - \Delta H_{CC,i}}{\varnothing_i \times \Delta H^0_{m,i}} \right) \times 100 \quad (1)$$

where $\Delta H_{m,i}$ and $\Delta H_{cc,i}$ are the melting and cold crystallization enthalpies obtained by DSC for the polymer *i*, respectively, ϕ_i is the mass fraction of the polymer *i*, and $\Delta H^0_{m,i}$ is the melting enthalpy of the 100% crystalline *i* polymer (93 J/g for PLA[36] and 109 J/g for PHBV[37]).

2.3.5. Mechanical characterization

The uniaxial tensile tests of the films were performed using an Instron universal testing machine (model 5569), equipped with a 500 N load cell, at room temperature and with a strain rate of 12.5 mm/min, following the specifications of ASTM D882-18[38]. The results for ultimate tensile strength (UTS), elongation at break (ε_b), and elastic modulus (E) were statistically analyzed by ANOVA (analysis of variance) and Tukey test, at a significance level of 0.05.

2.3.6. Water vapor permeability

The water vapor transmission rate (WVTR) of the films was measured according to the ASTM E96/E96M-24a standard[39], under humidity of 52%, using calcium chloride ($CaCl_2$) as a desiccant and magnesium nitrate ($Mg(NO_3)_2$) as a humidity controller. All samples (B, N, HC3, and HC5) were analyzed in triplicate. The WVTR was calculated using Equation 2:

$$WVTR = \frac{\left(G/t\right)}{A} \quad (2)$$

where G is the steady state weight change, t is the time during which G occurred, $\left(G/t\right)$ is the slope of the straight line on the curve of mass variation as a function of experiment time, and A is the test area (cup mouth area).

The water vapor permeability (P_{WV}) was obtained using Equation 3:

$$P_{WV} = \frac{WVTR}{\Delta p} \times e \quad (3)$$

where Δp is the vapor pressure difference and *e* is the thickness of the film. The P_{WV} values were statistically analyzed by ANOVA (analysis of variance) and Tukey test, at a significance level of 0.05.

2.3.7. Antimicrobial disk diffusion test

For the microbiological test, the microorganism *Escherichia coli* ATCC 25922 (Gram-negative) was used. Suspensions of this microorganism were prepared in saline solution until

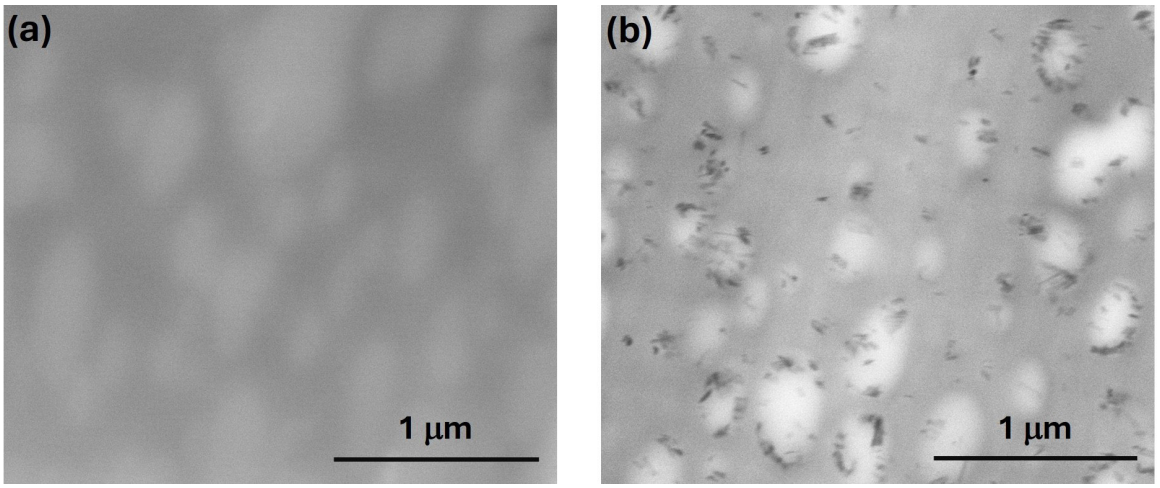

Figure 1. STEM micrographs of the (a) PLA/PHBV blend and (b) PLA/PHBV/SEP nanocomposite.

reaching a turbidity like the standard suspension (McFarland scale). The suspension was then spread using a sterile swab onto Petri dishes containing Mueller-Hinton agar, which had been previously prepared and solidified. The film samples were then cut into discs and placed on the surface of the inoculated agar. The plates were incubated in an oven at 37 °C for 24 hours. After this period, the plates were analyzed for the formation of inhibition zones. The test was performed in triplicate.

3. Results and Discussion

3.1. Morphology

To investigate the preferential localization of SEP in the PLA/PHBV blend, as well as its dispersion state and potential interfacial compatibilizing effect, STEM analyses were performed on samples of the PLA/PHBV blend (B) and the PLA/PHBV/SEP nanocomposite (N). The results are shown in Figure 1.

The PLA/PHBV blend, Figure 1 (a), exhibits a dispersed-phase morphology, with approximately spherical domains with an average diameter of 0.7 ± 0.2 µm. The mixing protocol used for nanocomposite preparation (involving the prior formation of a PHBV/SEP masterbatch followed by dilution in the PLA matrix) led to the preferential localization of SEP particles at the blend interface, Figure 1 (b). In this case, the spherical shape of the dispersed phase was preserved, but with reduced variability and a significant decrease in the average domain diameter (to 0.3 ± 0.1 µm). These findings suggest a reduction in interfacial energy and inhibition of coalescence of the dispersed phase, indicating a morphological stabilization effect and, consequently, an interfacial compatibilizing action of SEP in the PLA/PHBV blend.

3.2. Rheology

The influence of the inclusion of SEP and ZnO particles on the steady state rheological behavior of the PLA/PHBV blend at low shear rates is shown in Figure 2.

The addition of SEP to the blend led to a transition in the polymers' behavior, with viscosity increasing from

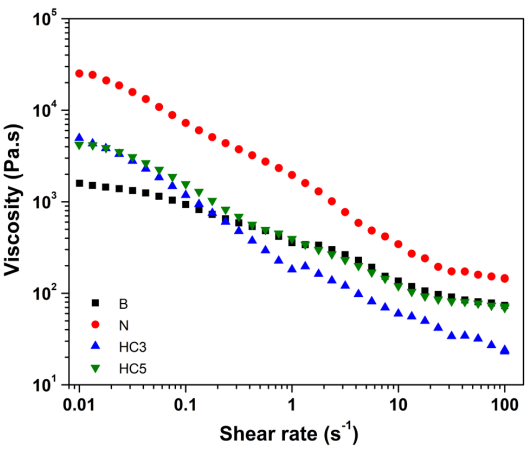

Figure 2. Viscosity as a function of shear rate for the PLA/PHBV blend (B) and its composites with SEP (N) and SEP/ZnO (HC) at 180°C.

1,450 Pa.s (sample B) to 21,130 Pa.s (sample N) at a shear rate of 0.01 s^{-1}. Up to approximately 0.1 s^{-1}, the PLA/PHBV blend (B) exhibited behavior closer to Newtonian, showing only a slight variation in viscosity as the shear rate increased. However, the increased macromolecular entanglement due to particle-particle interactions and polymer-particle interactions, facilitated by the -OH groups on the SEP surface and the ester groups of the polymers, induced the pseudoplastic behavior at lower shear rates in the PLA/PHBV/SEP nanocomposite (N). Similar behavior was observed when montmorillonite (MMT) was used as a reinforcing agent in the PLA/PHBV (75/25 wt/wt) blend[40]. At the lowest shear rates analyzed, the hybrid composites (samples HC3 and HC5) exhibited viscosities at least three times higher than that of the blend (B), but approximately five times lower than that of the SEP-based nanocomposite (N). While the presence of SEP nanoparticles contributed to increased viscosity compared to the PLA/PHBV blend, this effect may have been mitigated by PLA degradation in the presence of ZnO. Metal oxides, such as ZnO, can significantly degrade PLA macromolecules,

leading to reduced viscosity and thermomechanical properties. According to Murariu et al.[31], at elevated temperatures, zinc compounds catalyze intermolecular transesterification and depolymerization reactions in PLA, reducing its molar mass. Anžlovar *et al.* [41] conducted a comparative study on the degradation of PLA/ZnO and PHBV/ZnO composites produced via melt processing, finding that the incorporation of nanometric ZnO significantly reduced the molar mass of PLA, while the molar mass of PHBV remained practically unchanged, highlighting the greater susceptibility of PLA to degradation in the presence of ZnO.

Figure 3 shows the results of the oscillatory rheological tests conducted on the PLA/PHBV blend and its composites.

The PLA/PHBV blend (B) exhibited a predominance of viscous (G") over elastic (G') behavior throughout the analyzed angular frequency range. Upon the addition of 5 phr of SEP, the behavior became predominantly elastic up to approximately 1 rad/s, confirming the increased restriction on molecular movement due to the presence and content of the nanoparticles, as well as their interaction with the polymer chains. After the addition of ZnO, both G' and G" of the hybrid composites were reduced to values lower than those observed for the blend. Similar results were reported by Ahmadzadeh et al.[42] for PLA/PCL (polycaprolactone) blends with ZnO, where reductions in complex viscosity and storage modulus were observed due to PLA degradation, which reduced its molar mass.

Despite the significant changes in the rheological behavior of the materials, the processing of the PLA/PHBV/SEP nanocomposite and PLA/PHBV/SEP/ZnO hybrid composites proved to be feasible by melt mixing. No significant changes were observed in the formability of the materials during compression molding, and thin, homogeneous films were subsequently obtained for all the compositions studied.

3.3. X-ray diffraction (XRD)

Figure 4 shows the XRD curves of the studied compositions, as well as pure SEP and ZnO.

In the diffractogram of the blend (B), two main peaks were identified at 2θ values of 13.6° and 17.1°, along with a pronounced amorphous halo. According to Kanda et al.[43], the halo is attributed to the amorphous nature of PLA, while the peaks observed are characteristic of the orthorhombic unit cell of PHBV. Upon the addition of SEP (N), a new diffraction

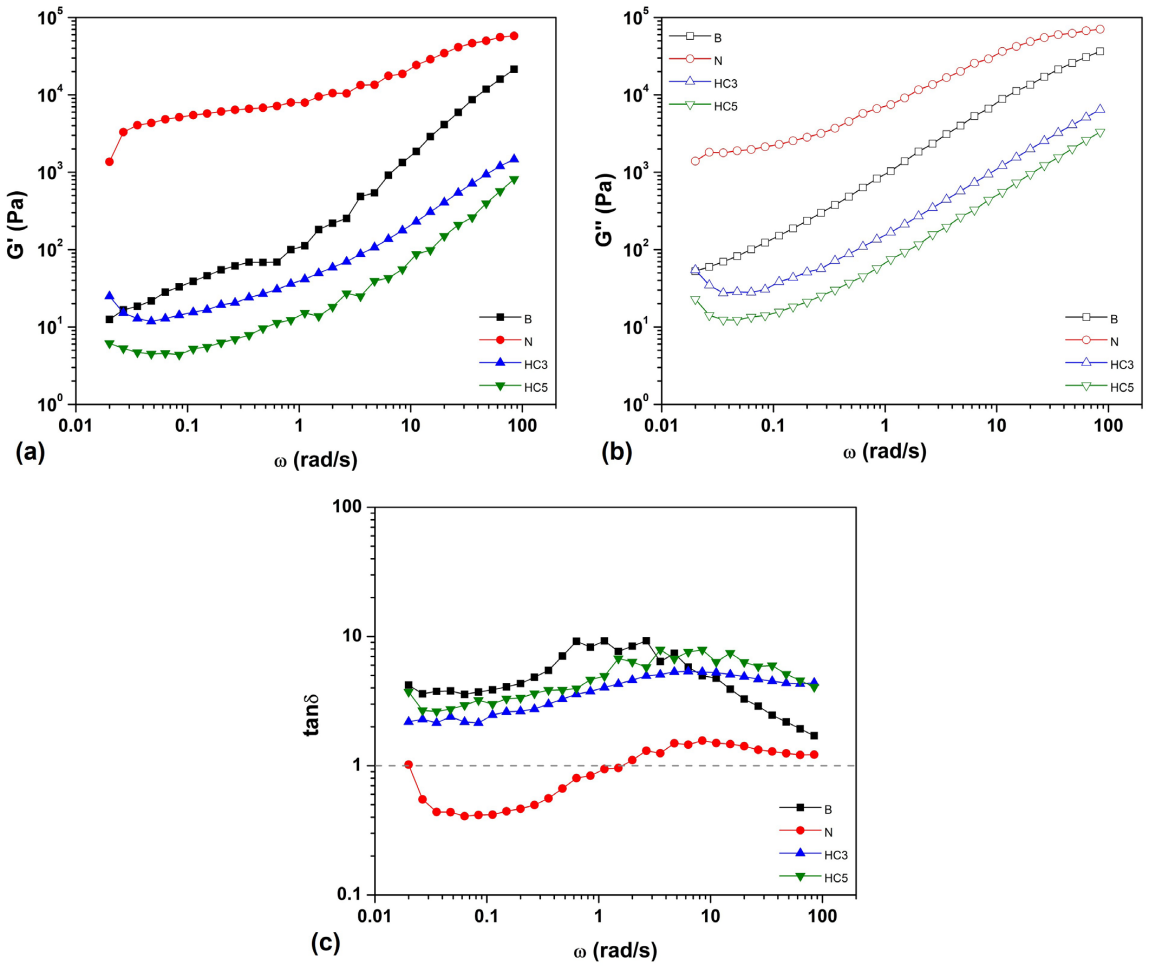

Figure 3. (a) Storage modulus, (b) loss modulus, and (c) tanδ as a function of frequency for the PLA/PHBV blend (B) and its composites with SEP (N) and SEP/ZnO (HC) at 180°C.

peak at 2θ = 7.2° was observed, which is characteristic of SEP in its natural and hydrated form[8]. The presence of hydroxyl groups on the surface of SEP needles can facilitate chemical interactions with biopolyesters, such as those in the blend[22]. The hybrid composites (HC) exhibited new peaks at 2θ values of 31.7°, 34.4°, 36.2°, 47.6°, 56.6°, 62.8°, and 68.1°, corresponding to the crystallographic planes (100), (002), (101), (102), (110), (103), and (112) of zinc oxide[44]. As the ZnO content increased from 3 phr to 5 phr, these peaks became more prominent. The XRD results confirmed the effective incorporation of SEP and ZnO into the composites and demonstrated that no significant structural changes occurred in the materials after the processing steps.

3.4. Thermal characterization

The thermal stability of SEP nanoparticles, ZnO particles, and the composites was evaluated by thermogravimetric analysis (TGA), and the results are presented in Figure 5 and Table 2.

Regarding SEP, as shown in Figure 5 (a), four thermal events can be observed: i) an initial mass loss up to approximately 100 °C, attributed to the elimination of zeolitic water and moisture; ii) a second step between 110 °C and 300 °C (peak at 250 °C), attributed to the loss of half of the Mg-coordinated water followed by a structural modification (transformation to dehydrated sepiolite); iii) a third step between 340 °C and 630 °C (peak at 520 °C), related to the loss of the second half of the remaining Mg-coordinated water in the collapsed channels, producing anhydrous sepiolite; iv) the onset of a fourth thermal event, above 700 °C (not fully characterized due to the maximum temperature used in the test), representing the dehydroxylation process of the octahedrally coordinated hydroxyl groups[45]. At 800 °C, a residue of approximately 91 wt% was obtained.

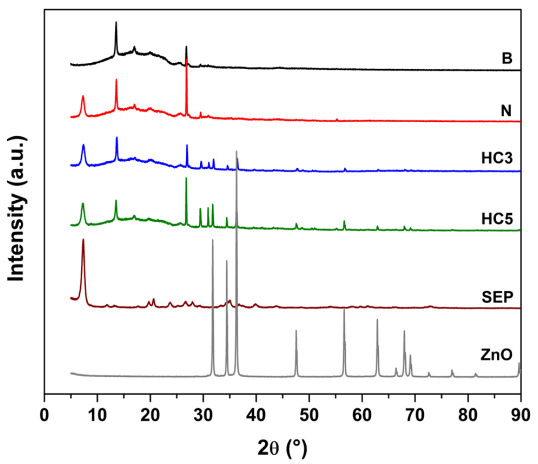

Figure 4. XRD patterns of zinc oxide (ZnO), sepiolite (SEP), PLA/PHBV blend (B) and its composites with SEP (N) and SEP/ZnO (HC).

The results obtained for ZnO, Figure 5 (a), demonstrate remarkable thermal stability, with only a small mass loss observed in the range of 395 °C to 460 °C (peak at 439 °C), and a residue of 99.7 wt% at 800 °C. This highlights the stability of this antimicrobial agent at temperatures typically used during the processing of thermoplastics in the molten state - a distinct advantage compared to other potential organic agents such as essential oils, organic acids, and enzymes, whose practical applicability is significantly limited by their low decomposition temperatures[46].

The thermal decomposition of the PLA/PHBV blend (B), as shown in Figure 5 (b and c), is characterized by two mass-loss steps[47]. The first step (I) corresponds to the PHBV phase, with a 35 wt% mass loss and a maximum decomposition rate at 305 °C. The thermal decomposition of PHBV follows a random chain scission mechanism involving a β-hydrogen elimination process, leading to the formation of substrate olefins and oligomers[48,49]. The second step (II) corresponds to the PLA matrix, with a 64 wt% mass loss and a peak temperature of 376 °C. PLA decomposition occurs through cleavage of the polymer backbone, resulting in the release of gaseous products such as cyclic oligomers, acetaldehyde, lactide, and carbon monoxide[50,51]. The incorporation of SEP (N), as depicted in Figure 5 (b and c), did not significantly affect the thermal stability of the blend. The initial (T_i) and final (T_f) decomposition temperatures for each polyester remained similar to those previously reported[47], while the residue percentage increased to 4.4 wt% due to the presence of the nanoparticle.

Conversely, the decomposition pattern of the hybrid composites (HC), shown in Figure 5 (b and c), is significantly affected by the presence and content of incorporated ZnO. The reduction in PLA molar mass is evident from the decreases in both T_i and T_f. Furthermore, the decomposition processes of the polymeric phases are no longer distinguishable, merging into a single mass-loss step corresponding to 85 wt%. The second thermal decomposition step for HC samples is much less pronounced, with mass losses ranging from 2 wt% and 3 wt%, likely associated with the decomposition of the incorporated particles. The observed residues for the hybrid composites are consistent with the SEP and ZnO contents in each composition.

Table 2. Mass loss values (Δm), initial (T_i) and final (T_f) decomposition temperatures, and residue at 800 °C obtained from TGA analyses of the PLA/PHBV blend (B) and its composites with SEP (N) and SEP/ZnO (HC).

Sample	Step I		Step II		Residue at 800 °C (wt%)
	Δm (%)	T_i / T_f (°C)	Δm (%)	T_i / T_f (°C)	
B	35.2	258 / 328	63.6	328 / 403	0.0
N	30.0	257 / 333	63.4	333 / 420	4.4
HC3	88.1	226 / 334	1.9	381 / 448	6.3
HC5	83.4	222 / 330	3.2	353 / 433	9.0

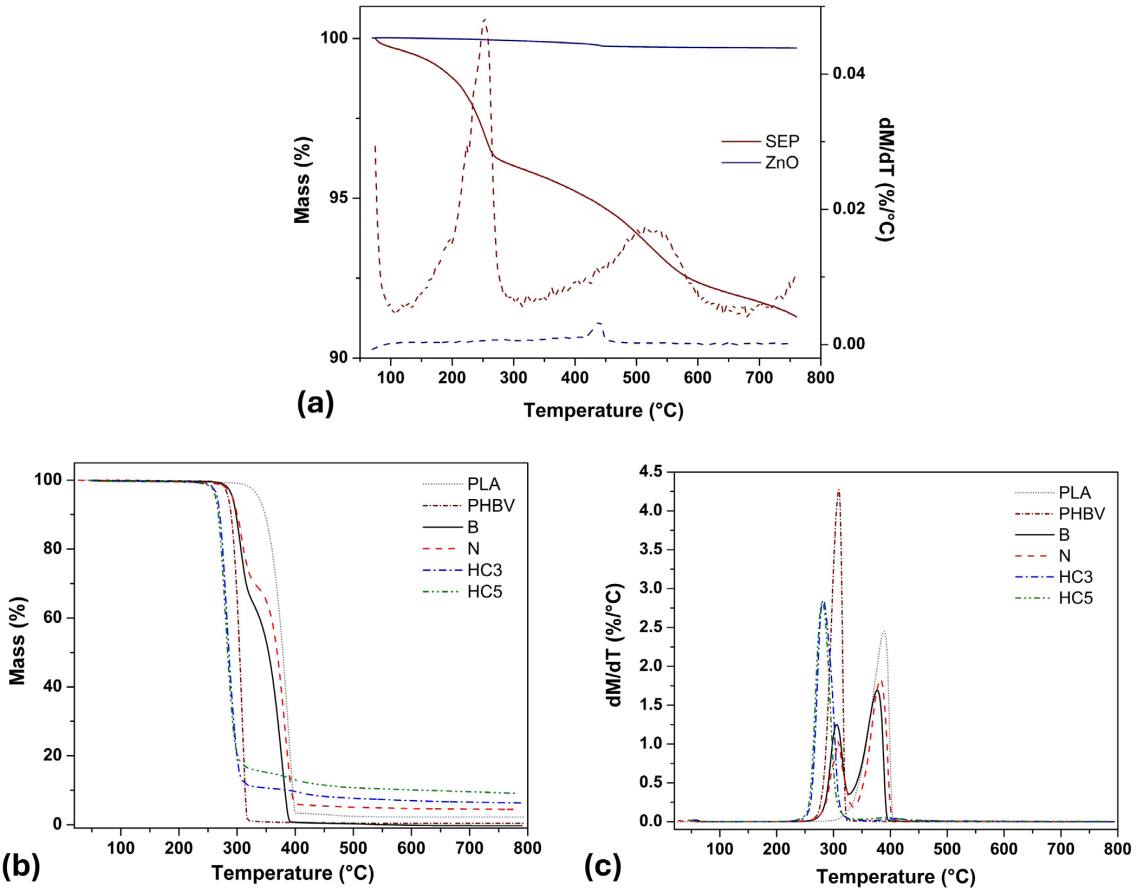

Figure 5. Thermogravimetric analysis of: (a) sepiolite and ZnO particles; (b and c) PLA, PHBV, PLA/PHBV blend (B) and its composites with SEP (N) and SEP/ZnO (HC).

The compression-molded films were characterized by DSC in the first heating cycle, and the obtained curves are presented in Figure 6. The observed thermal events (glass transition, $T_{g,PLA}$, cold crystallization, $T_{cc,PLA}$, and melting, $T_{m,PLA}$, temperatures of the PLA matrix, and the melting temperature, $T_{m,PHBV}$, of the dispersed PHBV phase) and the calculated degree of crystallinity of the polymeric phases ($X_{c,PLA}$ and $X_{c,PHBV}$) are summarized in Table 3.

The PLA/PHBV blend (B) exhibited a $T_{g,PLA}$ at approximately 60 °C, with a pronounced endothermic peak related to the relaxation of residual stress from the PLA molding process[36]. The $T_{g,PHBV}$ was not detected under the experimental conditions used but has been reported in other studies at around 0 °C[52]. An exothermic peak at 122 °C, corresponding to PLA cold crystallization was observed. Polymers with slow crystallization kinetics can acquire sufficient energy upon heating to organize into crystalline domains[53]. As the temperature increased, the melting of PLA crystals, primarily formed during heating, was observed at 149 °C, along with the melting of PHBV crystals at 171 °C.

The calculated X_c revealed differences in the crystallinity of the polymers in the blend. The presence of small amounts of D,D-lactide isomers hinders the crystallization process of PLA[54]. For PHBV, despite the addition of a small fraction of hydroxyvalerate (HV), which reduces its crystallinity degree compared to PHB[55], a $X_{c,PHBV}$ value near 70% was obtained, indicating high crystallinity degree for the dispersed phase of the blend.

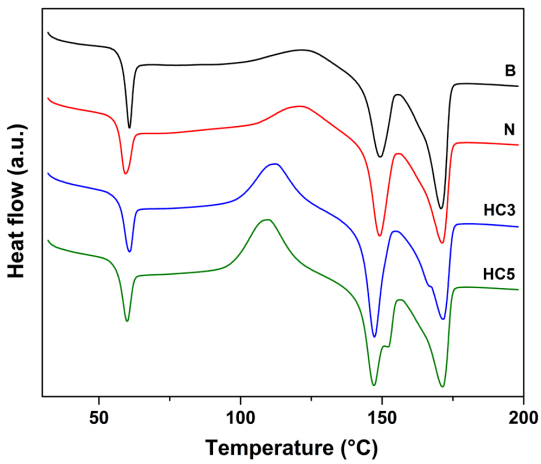

Figure 6. DSC curves from the first heating cycle of the PLA/PHBV blend (B) and its composites with SEP (N) and SEP/ZnO (HC).

Table 3. Values of glass transition (T_g), cold crystallization (T_{cc}), and melting (T_m) temperatures, and degree of crystallinity (X_c) of the polymeric phases, obtained during the first heating cycle of DSC for the films.

Sample	$T_{g,PLA}$ (°C)	$T_{cc,PLA}$ (°C)	$T_{m,PLA}$ (°C)	$T_{m,PHBV}$ (°C)	$X_{c,PLA}$ (%)	$X_{c,PHBV}$ (%)
B	60	122	149	171	6	70
N	59	121	149	171	0	64
HC3	61	112	148	172	0	66
HC5	60	110	147	171	0	67

After the inclusion of SEP (N), the thermal transitions reported for the blend were maintained. However, a slight reduction in X_c was noted for both polymeric phases. Similar behavior was observed by Fukushima et al.[15] for PLA nanocomposites with 7 wt% of SEP, attributing this to the presence of microaggregates of the needle-like clay mineral, which hindered the rearrangement of PLA macromolecules and reduced the formation of crystals.

In the hybrid composites (HC3 and HC5), a reduction of approximately 10 °C in the $T_{cc,PLA}$ was observed compared to samples B and N. The lower molar mass molecules formed during degradation in processing exhibit greater mobility, enabling the chains to organize into crystalline domains at lower temperatures[17]. However, this did not result in increased crystallinity, as shown in Table 3. Despite the melting of PLA and PHBV crystals occurring at temperatures close to those observed in the nanocomposite without ZnO, the melting pattern was subtly modified. Sample HC3 exhibited a shoulder on the melting peak of the PHBV phase, while HC5 showed a shoulder on the melting peak of the PLA matrix. Different melting peaks have been reported for PLA[56] and PHBV[57] and arise from the coexistence of distinct crystalline structures or crystals differing in size and/or levels of perfection.

3.5. Mechanical characterization

Figure 7 presents representative curves of the average stress-strain behavior obtained during the uniaxial tensile tests of the analyzed samples. The average values of ultimate tensile strength (UTS), elongation at break (ε_b), and elastic modulus (E) are summarized in Table 4.

All materials exhibited brittle fracture behavior, characterized by low values of elongation at break. The inclusion of SEP in the PLA/PHBV blend (sample N) resulted in a statistically significant increase in both ultimate tensile strength (UTS) and elastic modulus (E), while maintaining elongation at break. Despite evidence of some aggregation, as suggested by the DSC results, the nanoparticle´s morphology and high aspect ratio, combined with its interfacial location and strong adhesion and interaction with the polymers, optimized the mechanical performance of the nanocomposite, even without any surface treatment of the SEP. Moazeni et al.[58] reported that elastic modulus increases of up to 40% can be achieved with the incorporation of silane-treated SEP in PLA films, though this improvement often comes at the expense of reduced deformability in the polymer matrix.

For the hybrid composite containing 3 phr of ZnO (HC3), the tensile mechanical properties were statistically comparable to those of sample N, with a significant increase in UTS and E compared to the PLA/PHBV blend (sample B). In other words, despite the degradation observed during processing, the mechanical properties were not compromised but, on the contrary, were optimized relative to the blend. However, with a higher ZnO content (sample HC5), the effects of degradation became more pronounced, resulting in a UTS value similar to that of the blend and a reduction in ε_b.

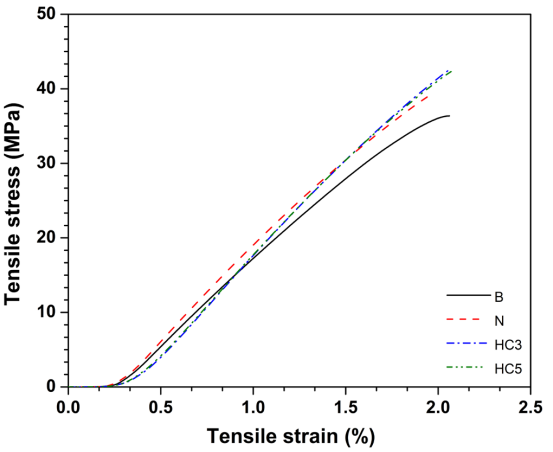

Figure 7. Representative curves of the average stress-strain behavior of the PLA/PHBV blend (B) and its composites with SEP (N) and SEP/ZnO (HC).

3.6. Water vapor permeability

In addition to thermal and mechanical properties, the gas barrier properties of a material are highly relevant for its performance in packaging applications, particularly in the food and healthcare sectors. The water vapor permeation behavior of the films developed in this work was analyzed, and the calculated water vapor permeability coefficients (P_{WV}), determined using Equation 3, are summarized in Table 4.

The P_{WV} of a polymeric compound depends on several factors, such as the chemical nature of the polymer and the penetrant, the polymer's morphology (especially its degree of crystallinity and molecular orientation), the shape and geometry of the particles present, and the presence of interfacial microvoids[59]. Generally, PLA is a bioplastic with a lower degree of crystallinity than PHBV and, consequently, exhibits a higher P_{WV}, as diffusion occurs more easily in amorphous phase of the polymer. Therefore, blending PHBV with PLA in appropriate concentrations can optimize its barrier properties[60]. The inclusion of particles typically increases the tortuous path for water vapor molecules to diffuse through the polymeric composite, thereby reducing P_{WV}. Inorganic particles are impermeable, forcing water molecules to move around them, which increases the path length needed to cross the sample

Table 4. Values of ultimate tensile strength UTS) and elongation (ε_b) at break, elastic modulus (E) and water vapor permeability (P_{WV}) for the films.

Sample	UTS (MPa)	ε_b (%)	E (GPa)	P_{WV} (10^{-7} g.m^{-1}.day^{-1}.Pa^{-1})
B	36.5 ± 2.2 $^{(B)}$*	2.1 ± 0.1 $^{(A)}$	2.5 ± 0.1 $^{(B)}$	3.6 ± 1.0 $^{(C)}$
N	42.1 ± 2.5 $^{(A)}$	2.1 ± 0.2 $^{(A)}$	2.7 ± 0.1 $^{(A)}$	7.9 ± 1.1 $^{(A)}$
HC3	44.2 ± 3.2 $^{(A)}$	2.2 ± 0.2 $^{(A)}$	2.9 ± 0.2 $^{(A)}$	4.3 ± 1.2 $^{(B,C)}$
HC5	35.8 ± 6.4 $^{(B)}$	1.7 ± 0.4 $^{(B)}$	2.9 ± 0.2 $^{(A)}$	7.2 ± 1.3 $^{(A,B)}$

* For each property analyzed, means that do not share a letter are significantly different, according to the Tukey test ($p < 0.05$).

and creates a tortuous pathway. The smaller the particle size, the more obstacles are created, further increasing the tortuous path. However, factors such as the surface hydrophilicity of SEP[61], the reduced X_c of the biopolyesters observed by DSC, interfacial microvoids, and the structural organization of SEP agglomerates forming tunnel-like channels may explain the increased P_{WV} of the PLA/PHBV/SEP nanocomposite (sample N) compared to the PLA/PHBV blend (sample B).

The P_{WV} of the HC3 hybrid composite was lower than that of the SEP nanocomposite and comparable to the blend, according to the statistical analysis performed. The inclusion of ZnO, a highly crystalline and impermeable inorganic filler, increased the tortuous path for penetrant molecules[62], counterbalancing the negative effects observed due to the presence of SEP. However, with a higher ZnO content (sample HC5), the P_{WV} values increased again, becoming statistically similar to those of sample N, indicating possible aggregation of the micrometric ZnO particles. It is also worth noting that, according to the DSC results, the crystallization pattern of the hybrid composites was altered. Thus, it cannot be ruled out that, in addition to a slight reduction in the degree of crystallinity, more defective crystals may have formed, which would also facilitate the diffusion process of the penetrant through the polymeric phases.

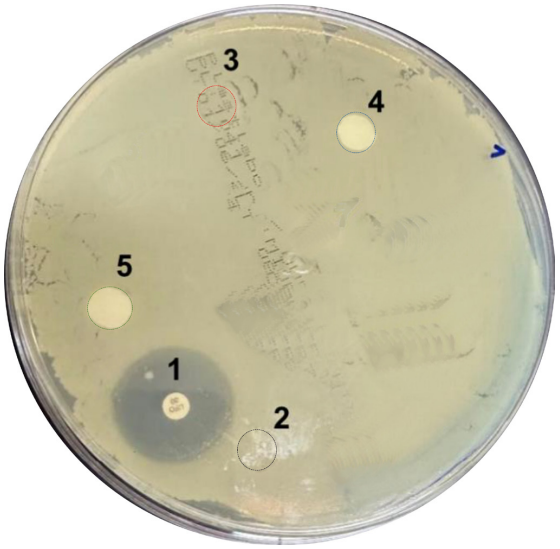

Figure 8. Results of antimicrobial tests by disk diffusion against *E. coli*: (1) CFO (cefoxitin, positive control); (2) B; (3) N; (4) HC3; (5) HC5. The edges of the analyzed films are highlighted in the image for better visualization.

3.7. Antimicrobial disk diffusion test

To assess the antimicrobial activity of ZnO microparticles against *Escherichia coli* (*E. coli*), a Gram-negative bacterial species, disk diffusion tests were performed using cefoxitin (CFO) as a positive control. Figure 8 presents a photograph of one of the sample sets analyzed after incubation at 37 °C for 24 h.

It is evident that CFO exhibited a significant inhibition halo, confirming the sensitivity of *E. coli* to the control antibiotic used. For all the samples analyzed, no visible growth of the bacterial species was observed on the surface of the films, indicating antimicrobial activity. However, no inhibition halo was observed around the hybrid composite samples, which did not display active behavior under the test conditions used.

The absence of an inhibition halo may be attributed to the physicochemical characteristics of the polyesters used to produce the hybrid composites, as well as the particle size of the ZnO and the test conditions. PLA has a T_g more than 20 °C above the test temperature, meaning its molecules are in the glassy state. Although the test temperature exceeds the T_g of PHBV, the material exhibits a high X_c (around 70%), which limits the diffusion of the metal oxide into the test medium. Furthermore, although nanosized ZnO particles are more effective as antimicrobial agents in polymeric composites[31], they also have a greater impact on the degradation of PLA[34,41]. Therefore, micrometric ZnO was chosen for this study to achieve an optimal balance between antimicrobial activity, processing performance, and the physicochemical properties of the hybrid composites. Doumbia et al.[63] and Pantani et al.[64], when producing filaments for the textile sector and films based on PLA/ZnO nanocomposites, respectively, reported variations in the sensitivity of bacterial strains tested using the minimum inhibitory concentration (MIC) assay. For example, the cytoplasmic membrane of Gram-negative bacteria contains lipopolysaccharides that can reduce permeability to certain chemical species. Additionally, the release of antimicrobial products, such as reactive oxygen species and Zn^{2+} ions, is often time dependent. According to the authors, achieving an effective minimum inhibitory concentration to prevent bacterial proliferation may require a period longer than 24 hours.

4. Conclusions

In this study, hybrid composites were developed via melt mixing followed by compression molding to produce films

with potential for multifunctional packaging applications. The composites were based on biodegradable polymers derived from renewable sources (PLA, PHBV), sepiolite (SEP) nanoparticles serving as both an interfacial compatibilizer for the polymer blend and a reinforcement agent, and micrometric ZnO particles as an antimicrobial agent.

The influence of the ZnO presence and content on PLA matrix degradation during processing was verified through rheological and thermal (TGA, DSC) analyses. However, no changes in processability or thermal stability were observed that would compromise the usability of the developed hybrid composites.

An optimized performance was observed for the hybrid composite containing 3 phr of ZnO (sample HC3), which demonstrated significant increases in ultimate tensile strength (UTS) and elastic modulus (E) without a reduction in deformation at break (ε_b) when compared to the PLA/PHBV blend (sample B). Furthermore, a reduction in water vapor permeability (P_{wv}) was noted compared to the nanocomposite containing only SEP (sample N). Above this ZnO content (sample HC5), more pronounced degradation of the polymer matrix and potential particle agglomeration led to a decrease in the overall performance of the composite.

Disk diffusion tests demonstrated activity against *E. coli* for all analyzed compositions, though without an active release of the antimicrobial agent.

In conclusion, the hybrid composite HC3 shows strong potential for producing films with optimized mechanical and permeation properties, as well as antibacterial activity. These characteristics make it suitable for use as biodegradable and antimicrobial multifunctional packaging produced through conventional melt-processing techniques for thermoplastics.

5. Acknowledgments

This work was supported by the Coordination for the Improvement of Higher Education Personnel - Brazil (CAPES) [Finance Code 001], the Brazilian National Council for Scientific and Technological Development (CNPq) [Grant Numbers 407288/2021-0, 161342/2021-3, INCT/Midas - 465594/2014-0, 116814/2023-3, and 116809/2023-0], and the Minas Gerais State Research Support Foundation (FAPEMIG) [INCT/Midas - Subproject 24998*26]. The authors also thank the Laboratory of Structural Characterization (LCE/DEMa/UFSCar) for the general facilities.

6. References

1. Fabra MJ, López-Rubio A, Lagaron JM. Biopolymers for food packaging applications. In: Aguilar MR, Román JS, editors. Smart polymers and their applications. Amsterdam: Elsevier; 2014. p. 476-509.
2. Law KL, Narayan R. Reducing environmental plastic pollution by designing polymer materials for managed end-of-life. Nat Rev Mater. 2022;7:104-16.
3. Rasal RM, Janorkar AV, Hirt DE. Poly(lactic acid) modifications. Prog Polym Sci. 2010;35:338-56.
4. Jost V, Kopitzky R. Blending of polyhydroxybutyrate-co-valerate with polylactic acid for packaging applications - reflections on miscibility and effects on the mechanical and barrier properties. Chem Biochem Eng Q. 2015;29:221-46.
5. Nofar M, Salehiyan R, Ray SS. Influence of nanoparticles and their selective localization on the structure and properties of polylactide-based blend nanocomposites. Compos, Part B Eng. 2021;215:108845.
6. Taguet A, Cassagnau P, Lopez-Cuesta JM. Structuration, selective dispersion and compatibilizing effect of (nano)fillers in polymer blends. Prog Polym Sci. 2014;39:1526-63.
7. Fenouillot F, Cassagnau P, Majesté JC. Uneven distribution of nanoparticles in immiscible fluids: morphology development in polymer blends. Polymer. 2009;50:1333-50.
8. Ruiz-Hitzky E. Molecular access to intercrystalline tunnels of sepiolite. J Mater Chem. 2001;11:86-91.
9. Tartaglione G, Tabuani D, Camino G. Thermal and morphological characterisation of organically modified sepiolite. Microporous Mesoporous Mater. 2008;107:161-8.
10. Coelho ACV, Santos PS. Argilas especiais: o que são, caracterização e propriedades. Quim Nova. 2007;30:146-52.
11. Yang F, Wang A. Recent researches on antimicrobial nanocomposite and hybrid materials based on sepiolite and palygorskite. Appl Clay Sci. 2022;219:106454.
12. Wu J, Zou X, Jing B, Dai W. Effect of sepiolite on the crystallization behavior of biodegradable poly(lactic acid) as an efficient nucleating agent. Polym Eng Sci. 2015;55:1104-12.
13. González A, Dasari A, Herrero B, Plancher E, Santarén J, Esteban A, et al. Fire retardancy behavior of PLA based nanocomposites. Polym Degrad Stabil. 2012;97:248-56.
14. Fukushima K, Tabuani D, Camino G. Nanocomposites of PLA and PCL based on montmorillonite and sepiolite. Mater Sci Eng C. 2009;29:1433-41.
15. Fukushima K, Tabuani D, Camino G. Poly(lactic acid)/clay nanocomposites: effect of nature and content of clay on morphology, thermal and thermo-mechanical properties. Mater Sci Eng C. 2012;32:1790-5.
16. Sabzi M, Jiang L, Atai M, Ghasemi I. PLA/sepiolite and PLA/calcium carbonate nanocomposites: a comparison study. J Appl Polym Sci. 2013;129:1734-44.
17. Fukushima K, Tabuani D, Abbate C, Arena M, Ferreri L. Effect of sepiolite on the biodegradation of poly(lactic acid) and polycaprolactone. Polym Degrad Stabil. 2010;95:2049-56.
18. Ajmal AW, Masood F, Yasin T. Influence of sepiolite on thermal, mechanical and biodegradation properties of poly-3-hydroxybutyrate-co-3-hydroxyvalerate nanocomposites. Appl Clay Sci. 2018;156:11-9.
19. Shakil O, Masood F, Yasin T. Characterization of physical and biodegradation properties of poly-3-hydroxybutyrate-co-3-hydroxyvalerate/sepiolite nanocomposites. Mater Sci Eng C. 2017;77:173-83.
20. Costa RC, Daitx TS, Mauler RS, Silva NM, Miotto M, Crespo JS, et al. Poly(hydroxybutyrate-co-hydroxyvalerate)-based nanocomposites for antimicrobial active food packaging containing oregano essential oil. Food Packag Shelf Life. 2020;26:100602.
21. Costa RC, Ineichen AP, Teixeira CS, Bellettini IC, Carli LN. Release of oregano essential oil from PHBV films in simulated food conditions. Polímeros. 2022;32:e2022028.
22. González-Ausejo J, Gámez-Pérez J, Balart R, Lagarón JM, Cabedo L. Effect of the addition of sepiolite on the morphology and properties of melt compounded PHBV/PLA blends. Polym Compos. 2019;40:E156-68.
23. Zembouai I, Kaci M, Zaidi L, Bruzaud S. Combined effects of sepiolite and Cloisite 30B on morphology and properties of poly(3-hydroxybutyrate-co-3-hydroxyvalerate)/polylactide blends. Polym Degrad Stabil. 2018;153:47-52.
24. Fadiji T, Rashvand M, Daramola MO, Iwarere AS. A Review on antimicrobial packaging for extending the shelf life of food. Processes. 2023;11:590.
25. Tawakkal ISMA, Cran MJ, Miltz J, Bigger SW. A review of poly(lactic acid)-based materials for antimicrobial packaging. J Food Sci. 2014;79:R1477-90.
26. Romero-Castelán E, Rodríguez-Hernández AI, Chavarría-Hernández N, López-Ortega MA, López-Cuellar MR. Natural

antimicrobial systems protected by complex polyhydroxyalkanoate matrices for food biopackaging applications: a review. Int J Biol Macromol. 2023;233:123418.
27. Oyama IMC, Anjos EGR, Morgado GFM, Martins EF, Passador FRP. Antistatic and antimicrobial packaging of PLA/PHBV blend-based graphene nanoplatelets nanocomposites. J Appl Polym Sci. 2023;140:e54484.
28. Anjos EGR, Brazil TR, Montagna LS, Morgado GFM, Martins EF, Pessan LA, et al. Biodegradation behavior and life cycle assessment of PLA/PHBV/Carbonaceous materials hybrid nanocomposites for antimicrobial multifunctional packaging. J Polym Environ. 2024;32:5098-114.
29. Min TT, Sun XL, Yuan ZP, Zhou LP, Jiao XY, Zha JW, et al. Novel antimicrobial packaging film based on porous poly(lactic acid) nanofiber and polymeric coating for humidity-controlled release of thyme essential oil. Lebensm Wiss Technol. 2021;135:110034.
30. Zende R, Ghase V, Jamdar V. Recent advances in the antimicrobial and antioxidant capabilities of PLA based active food packaging. Poly-Plast Tech Mat. 2025;64(4):439-64.
31. Murariu M, Doumbia A, Bonnaud L, Dechief AL, Paint Y, Ferreira M, et al. High-performance polylactide/ZnO nanocomposites designed for films and fibers with special end-use properties. Biomacromolecules. 2011;12:1762-71.
32. del Campo A, Lucas-Gil E, Rubio-Marcos F, Arrieta MP, Fernández-García M, Fernández JF, et al. Accelerated disintegration of compostable Ecovio polymer by using ZnO particles as filler. Polym Degrad Stabil. 2021;185:109501.
33. Murariu M, Dubois P. PLA composites: from production to properties. Adv Drug Deliv Rev. 2016;107:17-46.
34. Wang XJ, Huang Z, Wei MY, Lu T, Nong DD, Zhao JX, et al. Catalytic effect of nanosized ZnO and TiO2 on thermal degradation of poly(lactic acid) and isoconversional kinetic analysis. Thermochim Acta. 2019;672:14-24.
35. Backes EH, Pires LN, Costa LC, Passador FR, Pessan LA. Analysis of the degradation during melt processing of PLA/biosilicate composites. J Compos Sci. 2019;3:52.
36. Rodolfo MG, Costa LCC, Marini J. Toughened poly(lactic acid)/thermoplastic polyurethane uncompatibilized blends. J Polym Eng. 2022;42:214-22.
37. Vidhate S, Innocentini-Mei L, D'Souza NA. Mechanical and electrical multifunctional poly(3-hydroxybutyrate-co-3-hydroxyvalerate)-multiwall carbon nanotube nanocomposites. Polym Eng Sci. 2012;52:1367-74.
38. ASTM: American Society for Testing and Materials. ASTM D882-18 - Standard test method for tensile properties of thin plastic sheeting. West Conshohocken: ASTM International; 2018.
39. ASTM: American Society for Testing and Materials. ASTM E96/E96M-24a - Standard test methods for gravimetric determination of water vapor transmission rate of materials. West Conshohocken: ASTM International; 2024.
40. Zembouai I, Bruzaud S, Kaci M, Benhamida A, Corre YM, Grohens Y, et al. Synergistic effect of compatibilizer and Cloisite 30B on the functional properties of poly(3-hydroxybutyrate-co-3-hydroxyvalerate)/polylactide blends. Polym Eng Sci. 2014;54:2239-51.
41. Anžlovar A, Kržan A, Žagar E. Degradation of PLA/ZnO and PHBV/ZnO composites prepared by melt processing. Arab J Chem. 2018;11:343-52.
42. Ahmadzadeh Y, Babaei A, Goudarzi A. Assessment of localization and degradation of ZnO nano-particles in the PLA/PCL biocompatible blend through a comprehensive rheological characterization. Polym Degrad Stabil. 2018;158:136-47.
43. Kanda GS, Al-Qaradawi I, Luyt AS. Morphology and property changes in PLA/PHBV blends as function of blend composition. J Polym Res. 2018;25:196.
44. Kalpana VN, Kataru BAS, Sravani N, Vigneshwari T, Panneerselvam A, Rajeswari VD. Biosynthesis of zinc oxide nanoparticles using culture filtrates of Aspergillus niger: antimicrobial textiles and dye degradation studies. OpenNano. 2018;3:48-55.
45. Kok MV. Thermal characterization of sepiolite samples. Energy Sources Part A. 2013;35:173-83.
46. Espitia PJP, Soares NFF, Coimbra JSR, Andrade NJ, Cruz RS, Medeiros EAA. Zinc oxide nanoparticles: synthesis, antimicrobial activity and food packaging applications. Food Bioprocess Technol. 2012;5:1447-64.
47. Zhao H, Cui Z, Sun X, Turng LS, Peng X. Morphology and properties of injection molded solid and microcellular polylactic acid/polyhydroxybutyrate-valerate (PLA/PHBV) blends. Ind Eng Chem Res. 2013;52:2569-81.
48. Mofokeng JP, Luyt AS. Morphology and thermal degradation studies of melt-mixed poly(hydroxybutyrate-co-valerate) (PHBV)/poly(e-caprolactone) (PCL) biodegradable polymer blend nanocomposites with TiO_2 as filler. J Mater Sci. 2015;50:3812-24.
49. Nanda MR, Misra M, Mohanty AK. The effects of process engineering on the performance of PLA and PHBV blends. Macromol Mater Eng. 2011;296:719-28.
50. Rabelo LH, Munhoz RA, Marini J, Maestrelli SC. Development and characterization of PLA composites with high contents of a Brazilian refractory clay and improved fire performance. Mater Res. 2022;25:e20210444.
51. Biazin GG, Beatrice CAG, Augusto TA, Marini J, Costa LC. Quiescent and shear-induced non-isothermal crystallization kinetics of PLA/HNT nanocomposites. J Therm Anal Calorim. 2023;148:13463-85.
52. Gong J, Qiang Z, Ren J. In situ grafting approach for preparing PLA/PHBV degradable blends with improved mechanical properties. Polym Bull. 2022;79:9543-62.
53. Jandas PJ, Mohanty S, Nayak SK. Thermal properties and cold crystallization kinetics of surface-treated banana fiber (BF)-reinforced poly(lactic acid) (PLA) nanocomposites. J Therm Anal Calorim. 2013;114:1265-78.
54. Auras R, Lim LT, Selke SEM, Tsuji H, editors. Poly(Lactic Acid): synthesis, structures, properties, processing, and applications. Hoboken: John Wiley & Sons; 2010.
55. Kumar V, Sehgal R, Gupta R. Blends and composites of polyhydroxyalkanoates (PHAs) and their applications. Eur Polym J. 2021;161:110824.
56. Saeidlou S, Huneault MA, Li H, Park CB. Poly(lactic acid) crystallization. Prog Polym Sci. 2012;37:1657-77.
57. Meereboer KW, Pal AK, Misra M, Mohanty AK. Sustainable PHBV/cellulose acetate blends: effect of a chain extender and a plasticizer. ACS Omega. 2020;5:14221-31.
58. Moazeni N, Mohamad Z, Dehbari N. Study of silane treatment on poly-lactic acid(PLA)/sepiolite nanocomposite thin films. J Appl Polym Sci. 2015;132:41428.
59. Koros WJ, Moaddeb M. Gas barrier polymer. In: Salamone JC, editor. Polymeric materials encyclopedia. New York: CRC Press; 1996.
60. Zembouai I, Kaci M, Bruzaud S, Benhamida A, Corre YM, Grohens Y. A study of morphological, thermal, rheological and barrier properties of poly(3-hydroxybutyrate-co-3-hydroxyvalerate)/polylactide blends prepared by melt mixing. Polym Test. 2013;32:842-51.
61. Chen B, Jia Y, Zhang M, Li X, Yang J, Zhang X. Facile modification of sepiolite and its application in superhydrophobic coatings. Appl Clay Sci. 2019;174:1-9.
62. Tang Z, Fan F, Chu Z, Fan C, Qin Y. Barrier properties and characterizations of poly(lactic acid)/ZnO nanocomposites. Molecules. 2020;25:1310.
63. Doumbia AS, Vezin H, Ferreira M, Campagne C, Devaux E. Studies of polylactide/zinc oxide nanocomposites: influence of surface treatment on zinc oxide antibacterial activities in textile nanocomposites. J Appl Polym Sci. 2015;132:41776.

64. Pantani R, Gorrasi G, Vigliotta G, Murariu M, Dubois P. PLA-ZnO nanocomposite films: water vapor barrier properties and specific end-use characteristics. Eur Polym J. 2013;49:3471-82.

Data Availability

Research data is available upon request from the corresponding.